Supplemental Information

SNARE-Mediated Fusion of Single Chromaffin Granules with Pore-Spanning Membranes

Raphael Hubrich, Yongsoo Park, Ingo Mey, Reinhard Jahn, and Claudia Steinem

Supporting Information

SNARE-mediated fusion of single chromaffin granules with pore-spanning membranes

Raphael Hubrich[1], Yongsoo Park[2,3], Ingo P. Mey[1], Reinhard Jahn[2] and Claudia Steinem[1,4]*

[1]Institute of Organic and Biomolecular Chemistry, University of Göttingen, Tammannstr. 2, 37077 Göttingen, Germany; [2]Max-Plack-Institute for Biophysical Chemistry, Am Fassberg 11, 37077 Göttingen, Germany; [3]Department of Molecular Biology and Genetics, Koc University, Rumelifeneri Yolu 34450 Sarıyer, Istanbul, Turkey. [4]Max-Planck Institute for Dynamics and Self-Organization, Am Fassberg 11, 37077 Göttingen, Germany

1. Specificity of CG docking and fusion
2. Fusion of synthetic vesicles with PSMs
3. Diffusion analysis of synthetic vesicles and CGs on PSMs
4. Localizations of CGs on PSMs
5 Displacement filter to analyze CG mobility states
6. Probability density calculations of CG localizations

1. Specificity of CG docking and fusion

Movies S1A and B (zoom in of A) show typical fusion events of CGs labeled with DiD-C_{18} with a PSM composed of DOPC/POPE/POPS/cholesterol/PIP_2/Atto488-DPPE (48:19:10:20:2:1) and doped with the ΔN49 complex (p/l 1:500). The frame rate is 30 frames/s with scale bars of 5 µm.

The specificity of the events of CG docking and fusion on PSMs was proven by a control experiment, in which PSMs were prepared by spreading GUVs doped with blocked ΔN49 complex. Blocking was achieved by incubation of the ΔN49 complex with the soluble SNARE domain of synaptobrevin 2 (aa 1–96) prior to reconstitution. In the recorded time series neither docking nor fusion was observed (Fig. S1, Movie S2).
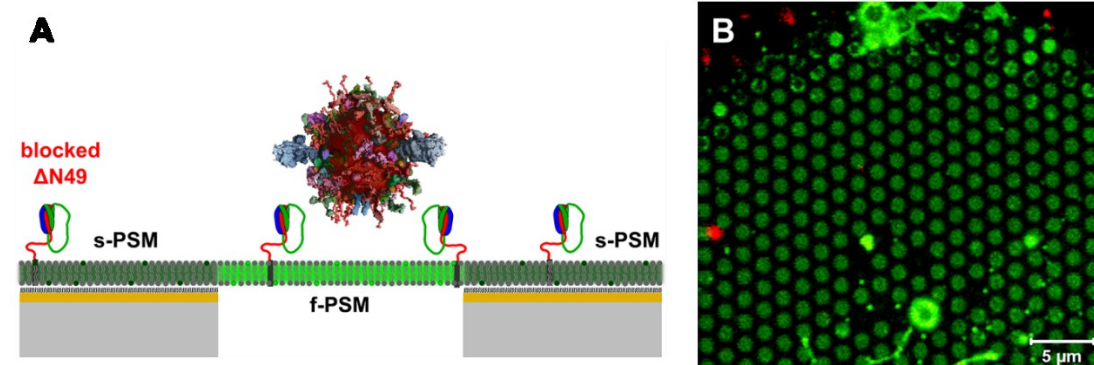

FIGURE S1 (*A*) Schematic illustration of the control experiment adding CGs to PSMs with blocked ΔN49 complex. (*B*) Snapshot of the control experiment (see Movie S2, 30 frames/s) showing CGs approaching the plane of the PSM. While no docking of CGs to the area covered by the PSM was monitored, non-specific adhesion to the membrane-uncovered surface was observed.

2. Fusion of synthetic vesicles with PSMs

For comparison, we performed a set of experiments, where we replaced labeled CGs by synthetic vesicles composed of DOPC/POPE/POPS/cholesterol/TexasRed-DPPE (50:19:10:20:1) and doped with synaptobrevin 2 (p/l 1:500). For the PSMs an identical lipid composition (DOPC/POPE/POPS/PIP$_2$/cholesterol/Atto488-DPPE, 48:19:10:2:20:1, doped with the ΔN49 complex (p/l 1:500) was used as for the CG fusion experiments. We evaluated 994 single fusion events to gather information about the fusion efficiency (Fig. S2A)
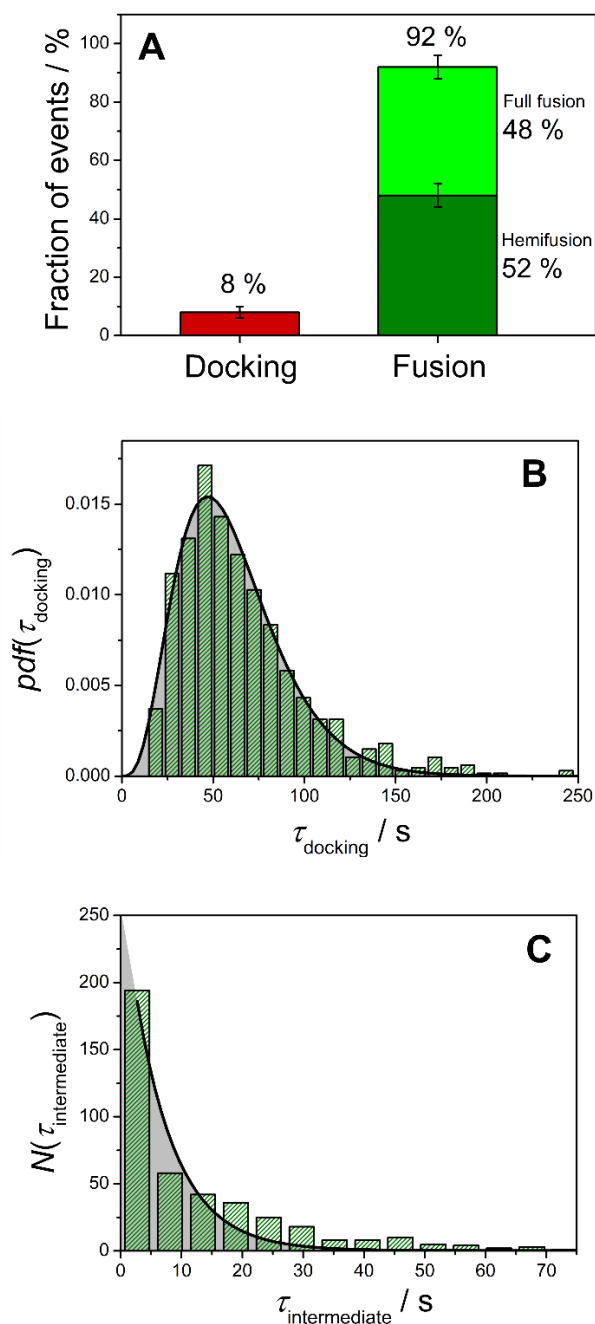

FIGURE S2 Statistical analysis of the fusion process of large unilamellar vesicles composed of DOPC/POPE/POPS/cholesterol/TexasRed-DPPE (50:19:10:20:1) and doped with synaptobrevin 2 (p/l 1:500) with PSMs composed of DOPC/POPE/POPS/PIP$_2$/cholesterol/Atto488-DPPE (48:19:10:2:20:1) and doped with the ΔN49 complex (p/l 1:500). (*A*) Fusion efficiency (*n* = 994). (*B*) Histogram of lifetimes of the docking state $\tau_{docking}$ (*n* = 769). The black line is the result of fitting eq. 1 to the data with k_1 = 0.074 ± 0.003 s^{-1} and *N* = 4.5 ± 0.2 resulting in an average docking lifetime of $\bar{\tau}_{docking}$ = 61 ± 5 s. (*C*) Histogram of the lifetimes of the intermediate states $\tau_{intermediate}$ (*n* = 425). Fitting eq. 2 to the data results in a rate constant of k_2 = 0.15 ± 0.02 s^{-1}.

3. Diffusion analysis of synthetic vesicles and CGs on PSMs

Diffusion coefficients of SNARE-bound particles on the distinct parts of the PSM (f- and s-PSM) were determined by tracking the particles followed by computing the MSD from the resulting trajectories (Figs. S3 and S4). We compared the diffusive behavior of CGs on PSMs with that of synthetic vesicles composed of DOPC/POPE/POPS/cholesterol/TexasRed-DPPE (50:19:10:20:1) and doped with synaptobrevin 2 (p/l 1:500) (Fig. S3).
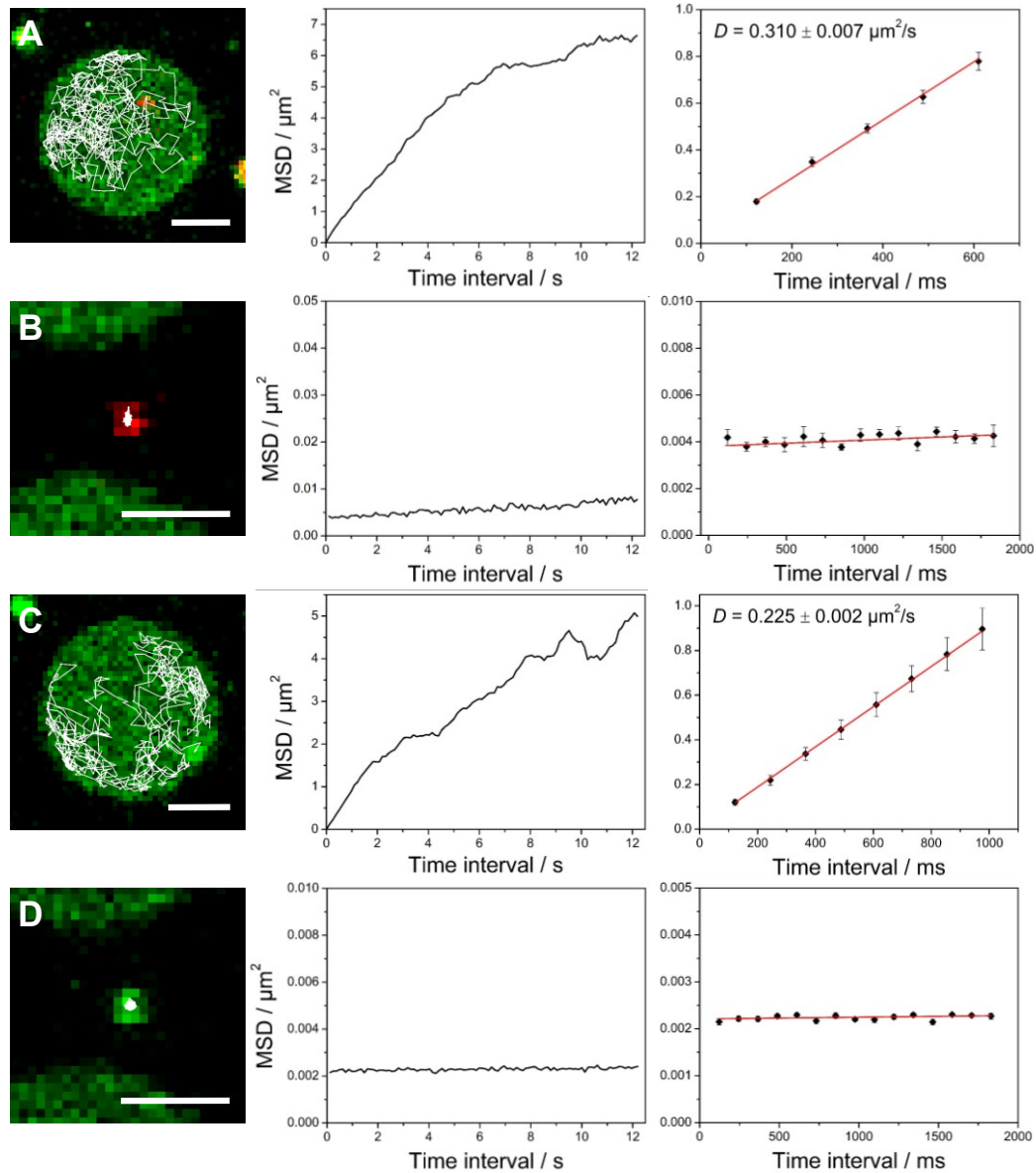

FIGURE S3 (*Left*) Fluorescence micrographs of synthetic vesicles composed of DOPC/POPE/POPS/cholesterol/TexasRed-DPPE (50:19:10:20:1) and doped with synaptobrevin 2 (p/l 1:500) with PSMs composed of DOPC/POPE/POPS/PIP$_2$/cholesterol/Atto488-DPPE (48:19:10:2:20:1) and doped with the ΔN49 complex (p/l 1:500). (*A/B*) before and (*C/D*) after the onset of lipid mixing together with the corresponding trajectories (white lines) obtained by single particle tracking. For both cases, pre- and post-lipid-mixing, an exemplary diffusion trajectory on the (*A/C*) f-PSM and (*B/D*) s-PSM is depicted; scale bars: 2 μm. (*Middle*) Plots of the respective, computed MSD against time intervals of up to 12 s. (*Right*) Diffusion coefficients *D* were obtained from the slope (4*D*) of MSD vs. time interval plots on shorter time scales.

Movies S3 and S4 show trajectories of CGs labeled with DiD-C$_{18}$ before (Movie S3) and after (Movie S4) lipid mixing with a PSM composed of DOPC/POPE/POPS/cholesterol/PIP$_2$/Atto488-DPPE (48:19:10:20:2:1) and doped with the ΔN49 complex (p/l 1:500). The frame rate is 30 frames/s. Fig. S4 shows representative trajectories and the corresponding MSDs.
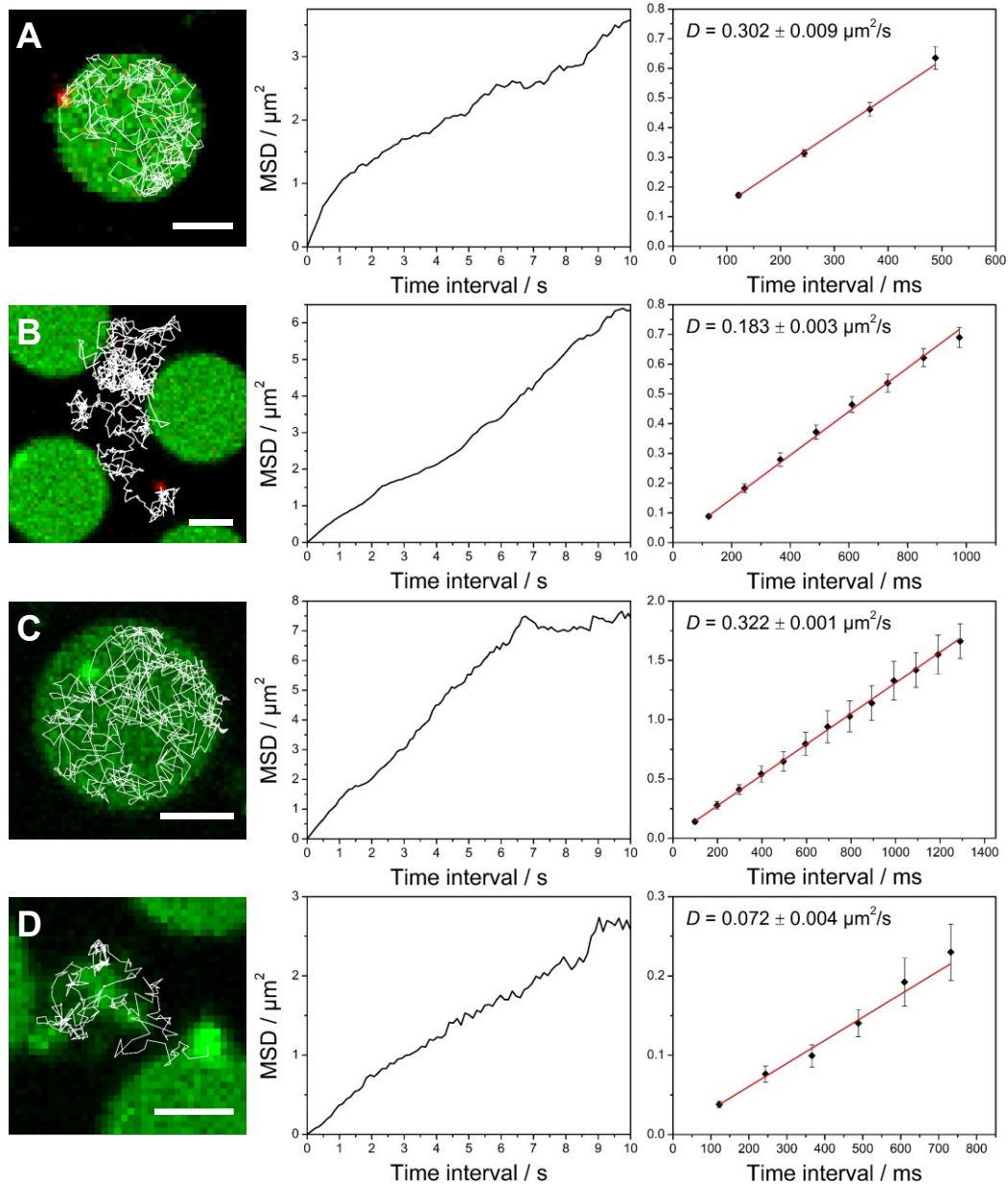
FIGURE S4 (*Left*) Fluorescence micrographs of mobile CGs on PSMs composed of DOPC/POPE/POPS/PIP$_2$/cholesterol/Atto488-DPPE (48:19:10:2:20:1) and doped with the ΔN49 complex (p/l 1:500) (*A/B*) before and (*C/D*) after the onset of lipid mixing together with the corresponding trajectories (white lines) obtained by single particle tracking. For both cases, pre- and post-lipid-mixing, an exemplary diffusion trajectory on the (*A/C*) f-PSM and (*B/D*) s-PSM is depicted; scale bars: 2 µm. (*Middle*) Plots of the respective, computed MSD against time intervals of up to 10 s. (*Right*) Diffusion coefficients *D* were obtained from the slope (4*D*) of MSD vs. time interval plots on shorter time scales.

4. Localizations of CGs on PSMs

For pre-lipid-mixing CG diffusion, 218 diffusion trajectories from 8 different time series were evaluated. In case of post-lipid-mixing CG diffusion, 45 trajectories from 9 different time series were analyzed. The histograms (Fig. S5) show the number of detected positions as a function on the PSMs.
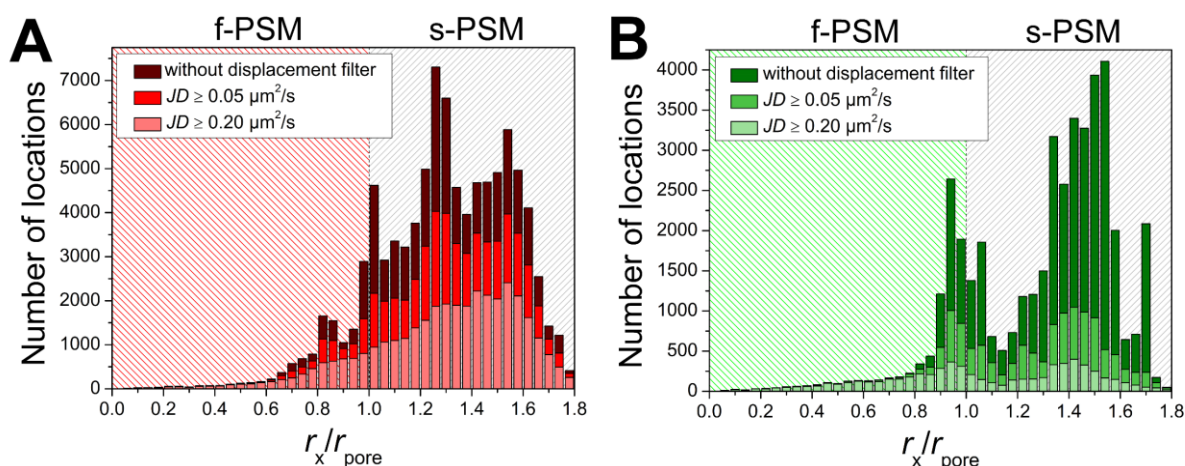
FIGURE S5 Histograms of relative pore center distances of diffusing CGs on PSMs. (*A*) Pore center distances of pre-lipid-mixing CG diffusion. The dark red bars display all determined CG-pore center distances, whereas the red and light red bars represent pore center distances of CGs with a jumping distance (*JD*) ≥ 0.05 µm²/s and *JD* ≥ 0.20 µm²/s, respectively. (*B*) Pore center distances of post-lipid-mixing CG diffusion. The dark green bars display all determined CG-pore center distances, whereas the green and the light green bars represent pore center distances of CGs with *JD* ≥ 0.05 µm²/s and ≥ 0.20 µm²/s, respectively.

5. Displacement filter to analyze CG mobility states

To have a closer look at CGs exhibiting a certain mobility state, two different displacement filters were applied. Two thresholds for the displacement of the CG's center of mass of 78 nm/122 ms and 156 nm/122 ms were set resulting in jumping distances of 0.05 µm²/s and 0.20 µm²/s, respectively.
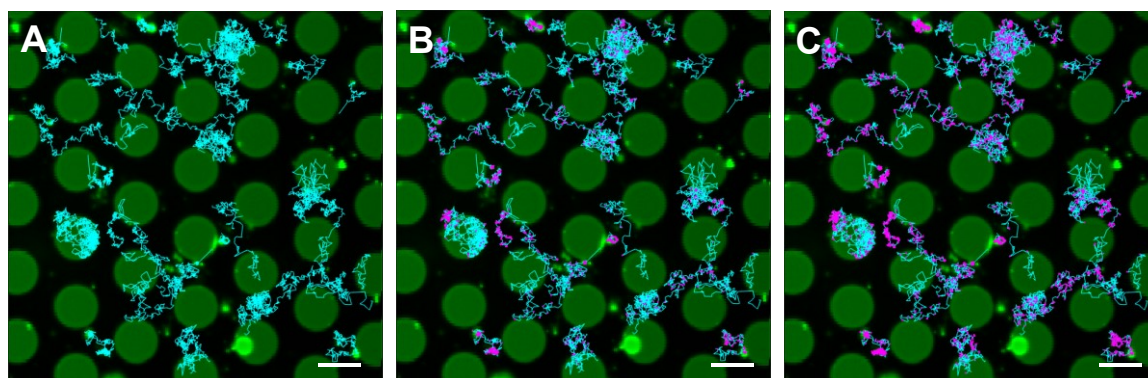

FIGURE S6 Illustration of CG diffusion trajectories before lipid mixing on PSMs (*A*) without a displacement filter and with a displacement filter excluding all CG locations either with a jumping distance (*B*) *JD* < 0.05 µm²/s or (*C*) *JD* < 0.20 µm²/s. The PSMs are shown in green, the trajectories in turquois and the excluded CG locations in magenta. Scale bars: 5 µm.

6. Probability density calculations of CG localizations

To calculate the probability density of positions of mobile CGs on the different parts of the PSM, the binned counts with a binning of Δr_x = 0.1 µm at position r_x were divided by the corresponding area segment A_x (Fig. S7).
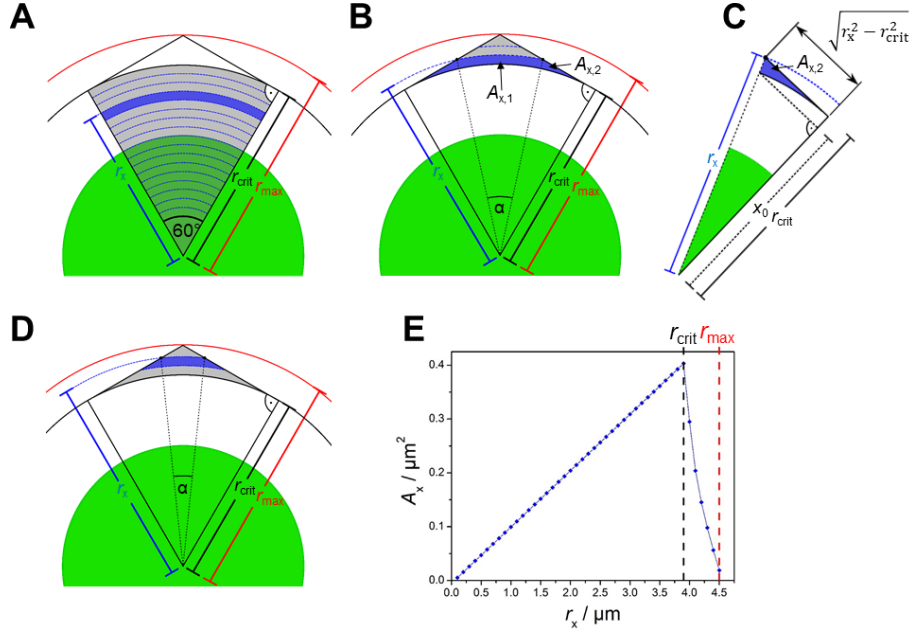
FIGURE S7 Schematic illustration to provide guidance for the derivation of the calculation of A_x. (*A*) Calculation of A_x as a function of r_x for 0.1 µm $\leq r_x \leq r_{crit}$. (*B-D*) Calculation of A_x as a function of r_x for $r_{crit} < r_x \leq r_{max}$. (*E*) Plot of A_x as a function of r_x. For the given pore geometry r_{crit} = 3.9 µm and r_{max} = 4.5 µm.

For 0.1 µm $\leq r_x \leq r_{crit}$ with $r_x = 0$ in the pore center, the area segments with an angle of 60° are calculated according to eq. S1 (Fig. S7A):

$$A_x(r_x) = \frac{1}{6}\left(\pi\, r_x^{\,2} - \pi\,(r_x - \Delta r_x)^2\right)$$ (S1)

For 4.0 µm $\leq r_x \leq r_{max}$ the circular segments of the three pores (see Fig. 7A) start to overlap and thus a non-centrosymmetric situation arises (Fig. S7B-D). The segment area is divided into two parts $A_{x,1}$ and $A_{x,2}$ (Fig. S7B). $A_{x,1}$ is given by eq. S2:

$$A_{x,1}(r_x) = \pi\left(r_x^2 - r_{crit}^2\right)\frac{\dfrac{\pi}{3} - 2\arccos\left(\dfrac{r_{crit}}{r_x}\right)}{2\pi}$$ (S2)

$A_{x,2}$ is given by the following integral (eq. S3):

$$A_{x,2}(r_x) = \int_{x_0}^{r_{crit}} \frac{\sqrt{r_x^2 - r_{crit}^2}}{r_{crit}}\, x - \sqrt{r_{crit}^2 - x^2}\, dx$$ (S3)

with $x_0 = r_{crit}^2 / r_x$. For r_x = 4.0 µm, $A_x(r_x) = A_{x,1}(r_x) + 2\,A_{x,2}(r_x)$, for $r_x > 4.0$ µm, $A_x(r_x) = A_{x,1}(r_x)$- $A_{x,1}(r_x-\Delta r_x) + 2\,(A_{x,2}(r_x)-A_{x,2}(r_x-\Delta r_x))$. Fig. S7E shows the result of the area segments A_x as a function of r_x.

By applying the displacement filter to the monitored CG diffusion trajectories, the normalized counts of r_x as well as the corresponding probability densities were determined for the three different mobility states of CG diffusion.